Analysis of In-Flight Winds for Shuttle Mission STS 51-L

GEORGE H. FICHTL,*,@ NATHANIEL D. REYNOLDS,†,‡ ALAN E. JOHNSTON,* STANLEY I. ADELFANG,††
WADE BATTS,†† LARRY LOTT,** PAUL J. MEYER,* ORVEL E. SMITH,†† MARION S. SWINT,*
AND OTHA H. VAUGHAN, JR.*

*Structures and Dynamics Laboratory, Marshall Space Flight Center, Alabama
**Systems Analysis and Integration Laboratory, Marshall Space Flight Center, Alabama
†Universities Space Research Association, Huntsville, Alabama
††Computer Sciences Corporation, Huntsville, Alabama

(Manuscript received 14 September 1987, in final form 19 February 1988)

ABSTRACT

Television photos of smoke plumes are analyzed to estimate meridional wind shear on the space shuttle Challenger associated with the accident of Mission 51-L. Gust velocities were obtained by detailed examination of the debris trails. The shuttle exhaust trail was used to establish altitudes of significant features in the photographs. Wind data obtained from the photographs compare favorably with data obtained from a rawinsonde released 9 min after the launch of the shuttle.

1. Introduction

This paper reports on a study to provide an independent estimate of the ascent winds associated with the Space Shuttle Mission STS 51-L incident. The study was performed to validate the rawinsonde wind observations initiated 9 min after launch. The rawinsonde data played a central role in the assessment of the dynamic loads experienced by 51-L during launch. Our study focuses on the meridional wind profile since the launch direction was due east and since crosswinds are a factor in assessing dynamic loads. Plume data from smoke trails associated with falling debris were used in this independent assessment of the ascent wind environment. The shuttle exhaust plume data was used to obtain a reference altitude that proved useful in establishing the altitudes of other significant features on the photographs.

During the prelaunch countdown, wind data are acquired at regular intervals for structural loads assessment using Jimspheres (Fichtl 1971 and Fichtl et al. 1972) tracked with the FPS-16 radar. Immediately after launch, standard procedures call for the additional launch of a Jimsphere to acquire a wind profile for postflight assessment. Due to the accident, the radars (FPS-16) normally used to track the Jimsphere were not available and therefore a rawinsonde wind profile measurement was initiated at 9 min after launch. Figure 1 provides the L + 9 minute rawinsonde wind profile, and Figs. 2 and 3 provide the zonal and meridional wind profiles from L − 4.5 h to L + 3.5 h acquired by rawinsonde and Jimsphere instrumentation. The flow is characterized by a westerly shear flow with maximum speed of 98 m s^{-1} for elevations between approximately 12 and 14 km. The mean wind direction at L + 9 min is 290° at 3.0 km, backing to 270° at 11.6 km and remaining near 270° up to 18.3 km. A description of the synoptic meteorological conditions for 51-L is given in Uccellini et al. (1986).

Figures 4 and 5 provide plan and vertical/east–west elevation views of the 51-L trajectory, location of the television sites from which the launch was observed, and location of the exhaust plume and the debris smoke trail used in the analysis. No attempt was made to triangulate (Tolefson and Henry 1961), since television camera pointing and zoom time histories were not available. Instead, individual pictures were analyzed.

The best panoramic views for analysis of the exhaust and debris smoke trails were provided by TV-2. The trails drifted to the south such that at 160–170 sec after failure a debris smoke trail was oriented directly east of site TV-2. The footprint area associated with this selected piece of debris at 169 sec after the explosion is indicated in Fig. 4. A schematic of this debris trail is shown in Fig. 5.

Our goal was to derive wind information from the debris smoke trail depicted in Fig. 6. The north–south deformation of these trails are caused by the vertical variation of the meridional winds and provides an opportunity to examine the meridional wind profile.

@ *Current assignment:* NASA Headquarters, Washington, D.C.
‡ *Current affiliation:* University of Alabama, Huntsville, Alabama
Corresponding author address: Dr. George H. Fichtl, Code MES, NASA Headquarters, Washington, DC 20547.

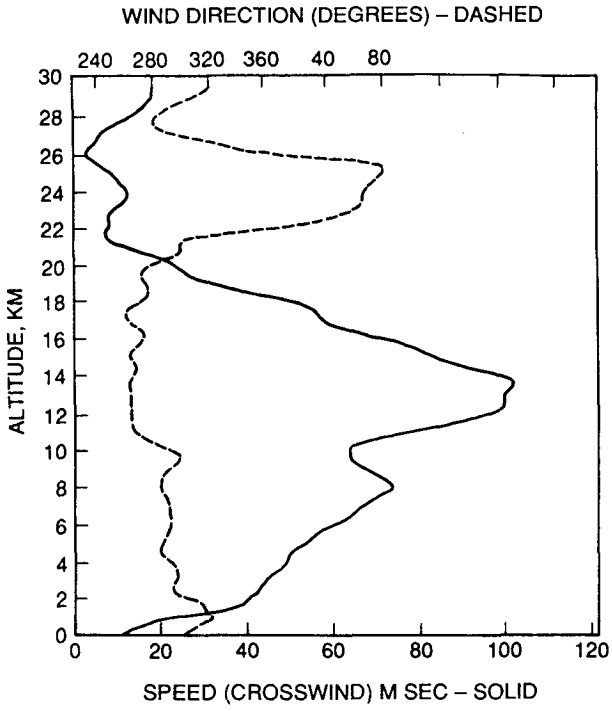

FIG. 1. The wind profile at 9 min after launch, as measured by a rawinsonde.

2. Meridional winds

Figure 7 provides the L + 9 min meridional wind profile as measured by the rawinsonde and the associated profile derived from the debris trail depicted in Fig. 6. Below approximately 11 km altitude, the meridional profile can be represented by a mean wind of 11.9 m s^{-1} with superimposed perturbations. Similarly, above approximately 11 km altitude, the meridional wind profile is characterized by a mean wind equal to -4.6 m s^{-1} with superimposed perturbations.

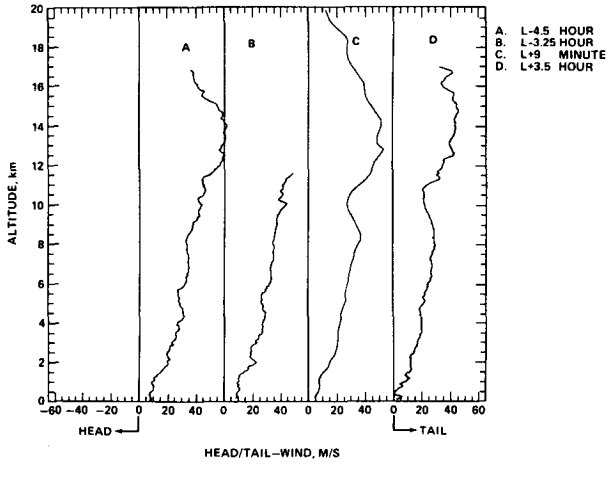

FIG. 2. Head/tail-wind profiles associated with 51-L; (a) Jimsphere profile 4.5 h before launch (L − 4.5 h), (b) Jimsphere profile at L − 3.25 h, (c) rawinsonde profile at L + 9 min, (d) Jimsphere profile at L + 3.25 h. For 51-L, a tail wind is a westerly wind.

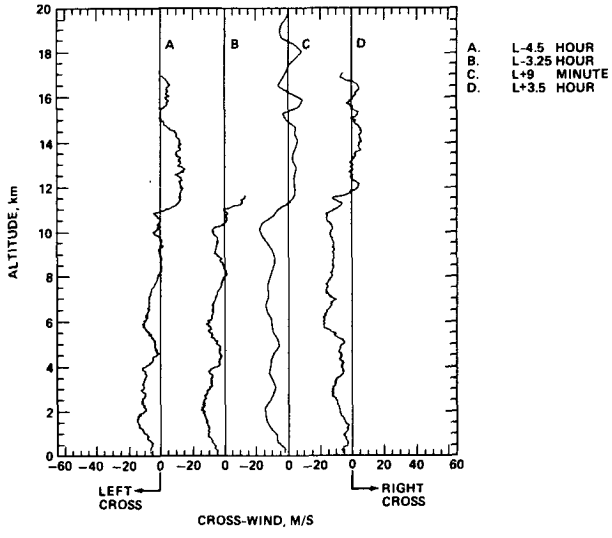

FIG. 3. Crosswind profiles associated with 51-L, measured in the same manner and at the same times as the corresponding profiles shown in Fig. 2. A right crosswind is a horizontal wind normal to the vehicle and blowing toward the right as seen by an observer in the orbiter, looking forward. For 51-L, a right crosswind is a southerly wind, due to the inverted attitude of the vehicle.

a. Debris trail trajectory analysis

The initial debris trajectory was essentially tangent to the flight path and the piece of debris in question was assumed to be ejected from the explosion with a velocity equal to the shuttle velocity (328 m s^{-1}) relative to the Earth. We assume the equations of motion of the debris can be represented in terms of a drag force and a gravitational body force, so that

$$\ddot{\mathbf{R}} = |\mathbf{V} - \dot{\mathbf{R}}|(\mathbf{V} - \dot{\mathbf{R}})/g\tau^2 - g\mathbf{k}, \qquad (1)$$

where $\mathbf{R}$ is the position vector of the debris particle relative to an earth-fixed frame of reference, $\mathbf{V}$ the wind vector, g and $\mathbf{k}$ have their usual meanings, and ($\dot{}$) denotes time differentiation. The quantity τ is a drag force time scale, given by

$$g\tau = (2mg/\rho AC_D)^{1/2}e^{\beta z/2}, \qquad (2)$$

with m, A, and C_D being the mass, characteristic cross-sectional area, and drag coefficient of the debris, ρ the atmospheric density at the earth's surface, β the reciprocal of the atmospheric density scale height for an isothermal atmosphere (with a value equal to 1.43 $\times 10^{-4}$ m^{-1}) and z the height above sea level in meters. The quantity $g\tau$ is the terminal velocity of the debris particle at altitude z. An initial estimate of τ at sea level, i.e.,

$$g\tau_0 = (2mg/\rho_0 AC_D)^{1/2} \qquad (3)$$

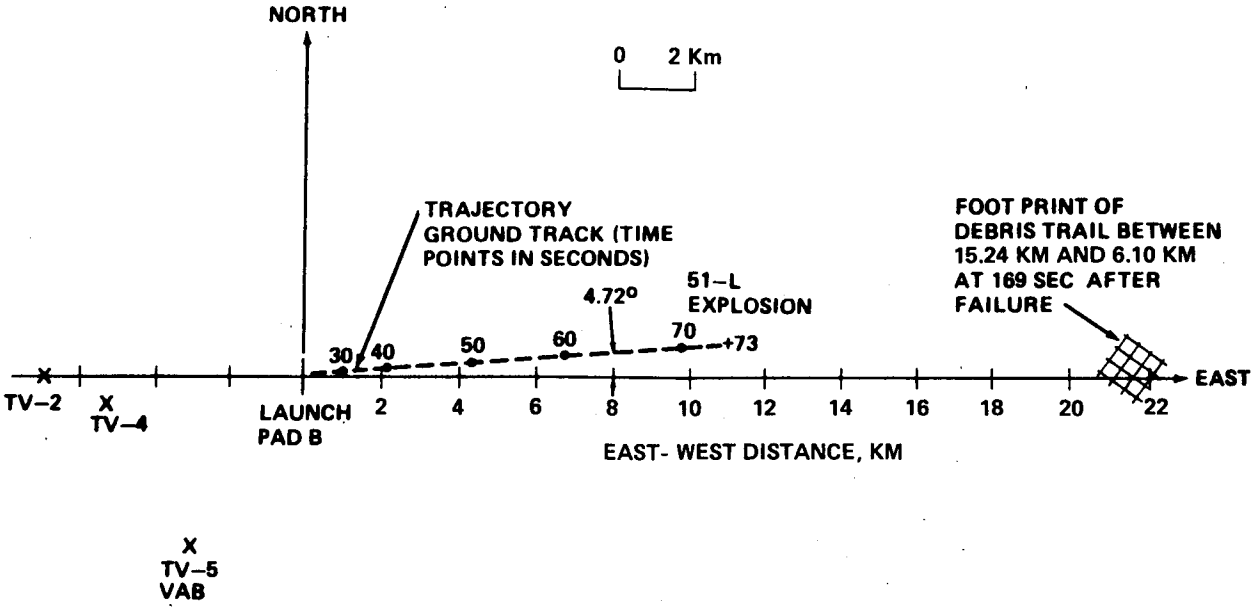

FIG. 4. The orientation of the television camera sites, the shuttle trajectory, and the debris trail at 169 sec after failure.

was assumed based on preliminary examination of debris smoke trail photographs. Equation (1) was used to estimate a trajectory of the selected piece of debris. This trajectory was used in our analysis to estimate the orientation of the debris smoke trail and location of the selected piece of debris at various times for selected television pictures when the selected debris particle was falling at terminal velocity. Revised estimates (described below) of the altitude of the debris particle derived from the television pictures were used to estimate the parameter τ_0 in Eq. (3). Equation (1), with the revised vertical variation of τ, was then used to estimate the trajectory shown in Figs. 4 and 5 for subsequent photographic analyses.

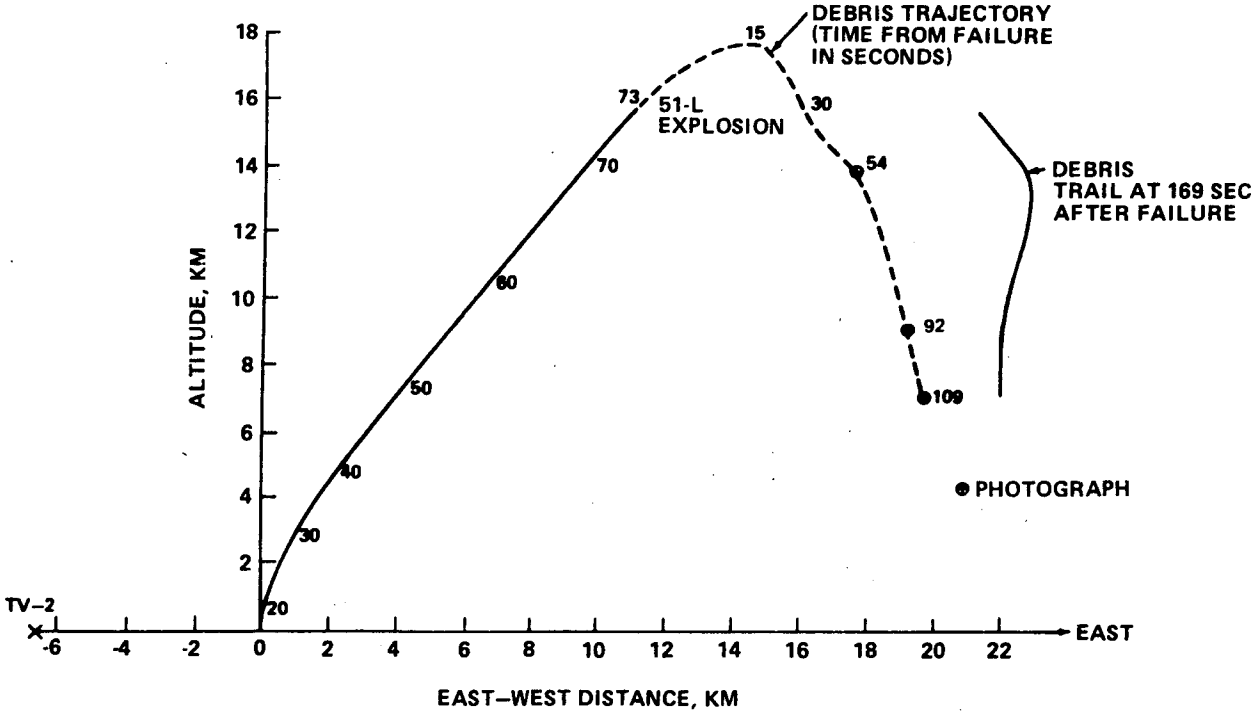

FIG. 5. A vertical/east–west view of the shuttle and debris trajectories.

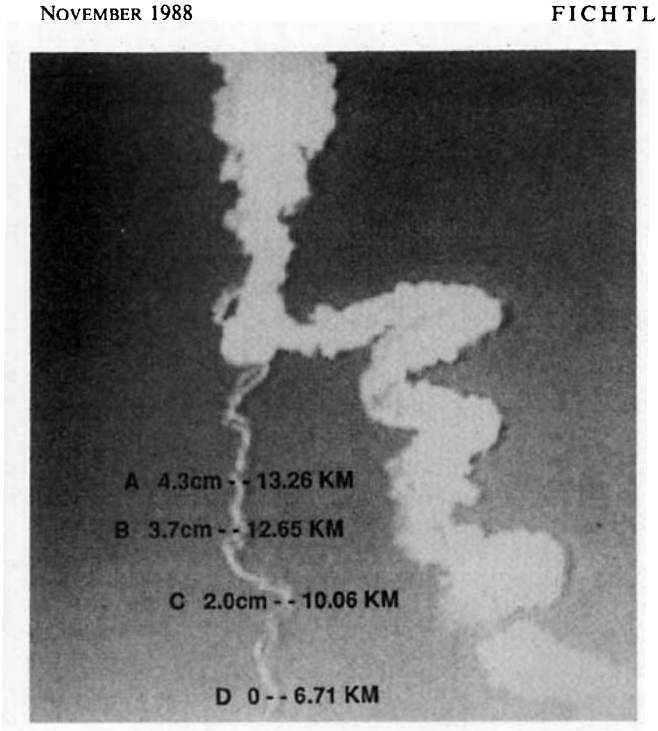

FIG. 6. A photograph of the shuttle exhaust cloud and debris trails from camera site TV-2 at 169 sec after failure, showing the points A, B, C, and D used in the debris trail data analysis.

Photographs of the subject debris trail at 54, 92, and 109 sec after failure (Figs. 8, 9, and 10) were used to obtain an estimate of τ_0. The altitude of the selected piece of debris is indicated by z_t. The altitudes z_B and z_r are altitudes that were used to derive a length scale to estimate z_t. The altitude z_B is equal to 11.28 km and was derived with a Computer-Aided Design/Computer-Aided Manufacturing (CAD/CAM) graphics system by matching the calculated centerline of the exhaust cloud (based on horizontal advection of the exhaust by the L + 9 min rawinsonde wind profile) with photographs of the exhaust cloud at various times after failure. (We estimate the rise of the plume due to buoyancy to be 500 m, which can be neglected.) The altitude $z_r = 15.24$ km is that for a bloblike feature on the exhaust cloud estimated to be approximately 300 m below the center of the conflagration, which is known from the vehicle trajectory time history. This feature persists for several minutes. Analysis of time of fall data from these figures yields $\tau_0 = 4.7$ s and the time of fall from 15.24 km as a function of altitude z given in Fig. 11.

b. Photographic analysis to determine debris altitudes

The photographs in Figs. 8, 9, and 10 were analyzed to determine the position of the selected piece of debris. We could have complete confidence in these positions if the piece of debris appeared in the images of two cameras optimally placed, if one had precise knowledge of the pointing directions, fields of view, focus, distortion, etc. for the cameras. Uncertainty was introduced by the unknown zoom adjustment of the camera. Therefore, the assumptions described below were introduced to analyze the photographs in Figs. 8, 9, and 10.

The vehicle exhaust trail from $z_B = 11.28$ km to altitude $z_r = 15.24$ km is assumed to be primarily advected by the westerly winds shown in Fig. 1. The initial horizontal position of the plume at altitude z is the vehicle trajectory $x = x_0(z)$ shown in Fig. 5. The angles above the horizon at camera site TV–2 for these points, i.e., z_B and z_r, are determined for each photograph by using the expressions

$$\alpha_r = \tan^{-1}(z_r/x_r), \tag{4}$$

$$\alpha_B = \tan^{-1}(z_B/x_B), \tag{5}$$

where horizontal location is given by

$$x = x_0(z) + u(z)[t_p - t_0(z)] + 6.71 \text{ km},$$

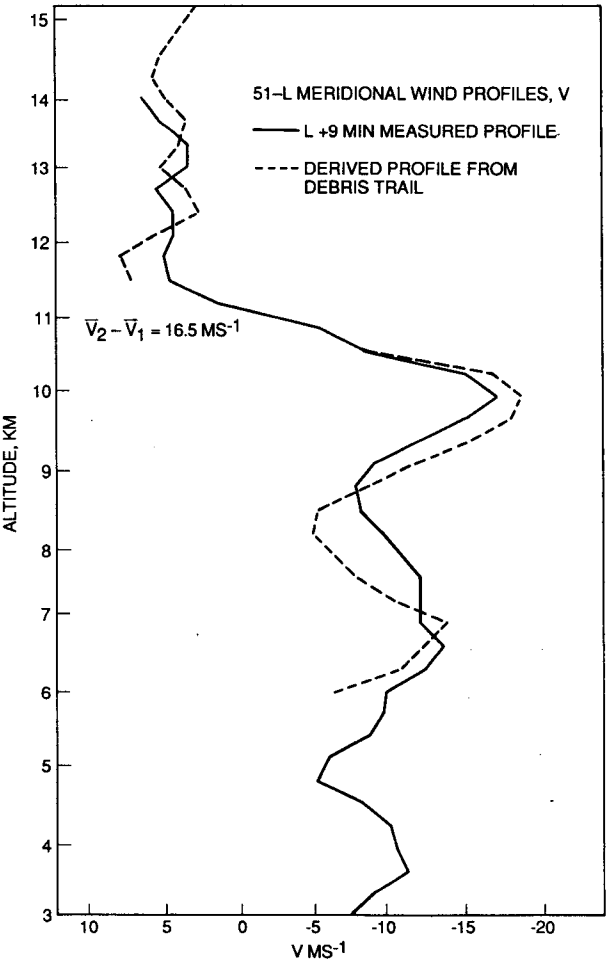

FIG. 7. A comparison of the L + 9 min rawinsonde wind profile and the debris-derived winds.

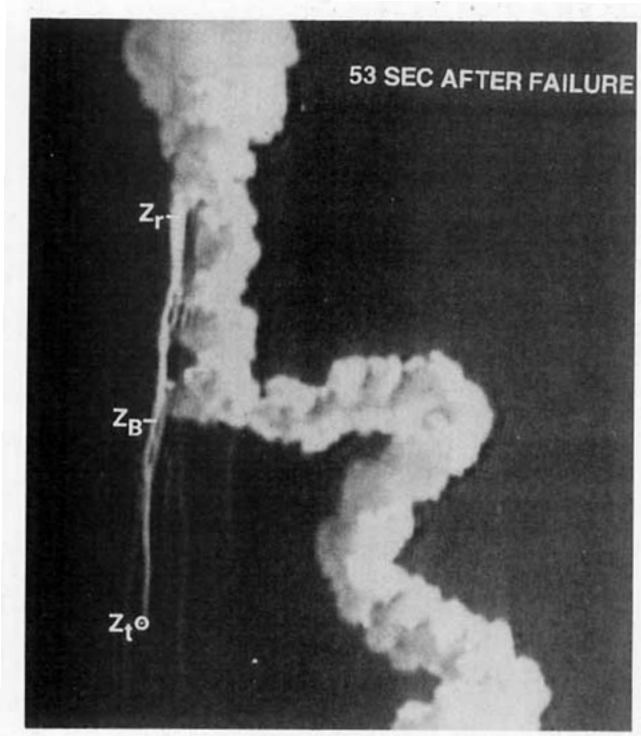

FIG. 8. A photograph of the shuttle exhaust cloud and debris trails at 53 sec after failure.

where t_p is the time of the photograph, $t_0(z)$ the time of generation of the portion of the exhaust trail at altitude z, and 6.71 km the distance from camera site TV-2 to the launch pad.

The optical axis is assumed to be at the center of the photograph. Once α_r and α_b are known, the angle α_{opt} between the optical axis and the horizontal, and, in turn, the angle to any feature of the photograph, can be determined. The positions on the photograph are proportional to the tangent of the angle from the optical axis to that feature; however, the angles encountered in this analysis are small enough so that the small angle approximation $\tan\alpha \approx \alpha$ can be used. In this manner, the angle of the piece of debris α_t above the horizon is determined. From the trajectory analysis, an x-value is obtained, and the height of the debris trail is computed using the relationship

$$z_t = (x_t + 6.71 \text{ km}) \tan\alpha_t. \qquad (6)$$

The debris position and angle information are given in Table 1.

3. Interpretation of debris trail data

In order to verify the linearity of the photograph in Fig. 6, points A, B, C, and D were identified, and the distance ratios AB/AD, AC/AD, BC/AD, and CD/AD were obtained independently for the photograph and the L + 9 min measured wind profile (Table 2). Based on the examination of the debris trail trajectory and the measured wind profile L + 9 min, it is concluded that points A, B, C, and D of Fig. 6 correspond to altitudes 13.26, 12.65, 10.06, and 6.71 km, which also correspond to the four peaks on the L + 9 min meridional wind profile at and below 13.26 km. Points A, B, and C are 4.3, 3.7, and 2.0 cm above point D in the original photograph used for Fig. 6. The distance ratios shown in Table 2 support the correspondence of features between the L + 9 min wind profile and the debris smoke trail.

The rawinsonde data in Fig. 7 suggest that the mean meridional wind can be represented as a two-layer model with mean wind equal to $v_1 = -4.6$ m s^{-1} above 11.28 km and mean wind equal to $v_2 = 11.9$ m s^{-1} below 11.28 km. We express the meridional wind profile for these layers as

$$v(z) = \bar{v}_1 + (\bar{v}_2 - \bar{v}_1)H(z) + v'(z) \qquad (7)$$

where the overbar denotes a vertical average in the respective layers, the prime denotes a departure from the average value, and

$$H(z) = \begin{cases} 1, & \text{if } z \geq 11.28 \text{ km}, \\ 0, & \text{if } z < 11.28 \text{ km}. \end{cases}$$

This model neglects the linear-like trend in the profile between 10.37 km and 11.28 km.

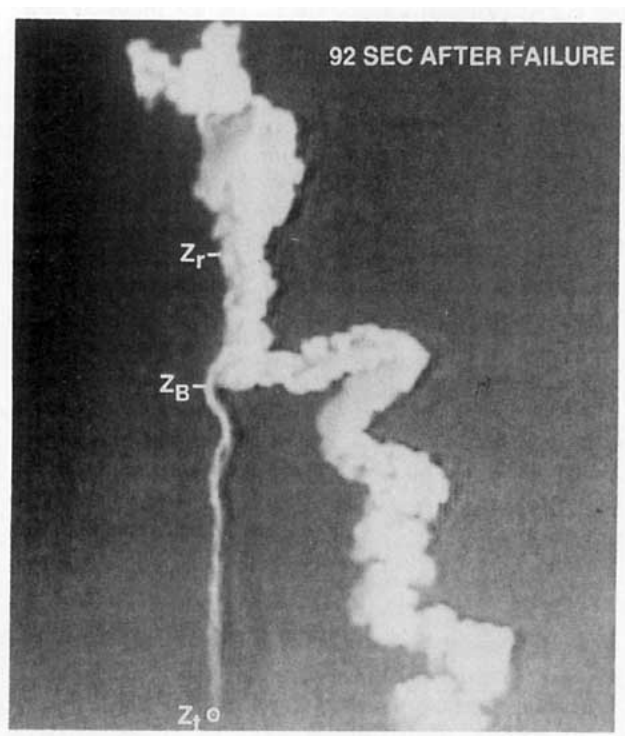

FIG. 9. A photograph of the shuttle exhaust cloud and debris trails at 92 sec after failure.

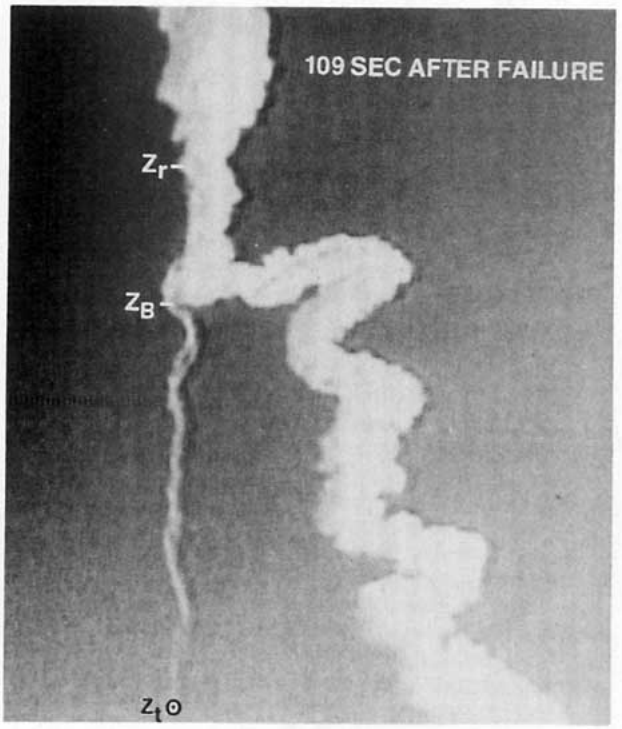

FIG. 10. A photograph of the shuttle exhaust cloud and debris trails at 109 sec after failure.

a. *Drift estimates*

The total drift of the smoke trail deposited at altitude z depicted in Fig. 6 is given by

$$D(z) = \int_0^{t_f(z)} \bar{v}(z'(t))dt + \int_0^{t_f(z)} v'(z'(t))dt + \int_{t_f(z)}^{t_p} v(z)dt, \quad (8)$$

where $t_f(z)$ is the time of fall to height z and is given in Fig. 11, $\bar{v}(z(t_f))$ the mean wind at altitude $z(t_f)$

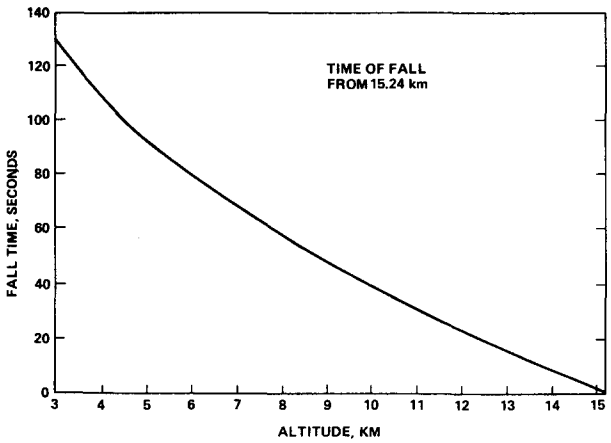

FIG. 11. The computed time of fall of a debris particle from 15.24 km.

TABLE 1. Pointing angles and calculated debris altitudes obtained from Figs. 8, 9, and 10.

Fig.	8	9	10
Time after failure (sec):	53	92	109
α_r (deg):	37.5	35.2	34.4
α_B (deg):	33.7	31.9	30.7
α_{opt} (deg):	32.7	30.1	26.5
α_t (deg):	29.4	22.0	18.0
z_t (km):	13.73	10.37	8.72

(which is the location of the piece of debris at fall time t_f referenced to 15.24 km altitude) and t_p the time of the photograph in Fig. 6. The first integral in Eq. (8) is the horizontal drift associated with the mean wind that occurs during fall to level z. The second integral is the drift during the fall to level z associated with the wind perturbation about the mean and is assumed to be sufficiently small compared to the drift associated with the mean wind. This assumes that the piece of debris has negligible response to the wind perturbations because the characteristic drag length scale $g\tau^2$ is sufficiently large compared to the wavelength λ of the wind perturbations $v'(z)$. That is, $\lambda/(g\tau^2) \leqslant 2$ for the horizontal velocity perturbation amplitude of the debris particle to be one-tenth or less of the gust velocity perturbation. The third term in Eq. (8) is the drift of the trail at level z after deposition of the smoke at that level and contains both the mean and perturbation meridional velocities.

Upon neglecting the second term on the right, Eq. (8) can be expressed as

$$D(z) = \bar{v}_1 t_p + H(z)(\bar{v}_2 - \bar{v}_1)(t_p - t_f(11.280 \text{ km})) + v'(z)(t_p - t_f(z)). \quad (9)$$

The first and second terms on the right side of Eq. (9) correspond to the mean displacement $\bar{D}(z)$ and the third term is the deviation about $\bar{D}(z)$, which we will refer to as $D'(z)$.

In deriving Eq. (9), it was assumed that the piece of debris adjusted instantaneously to the wind profile and we neglected the linear-like shear between 10.37 km and 11.28 km. Application of our dynamical model to the debris particle at and below 11.28 km yields a smoke trail drift correction of approximately −300 m. This bias error estimate was used to correct the mean drift calculations.

TABLE 2. Computed altitude ratios.

Ratio	L + 9 min meridional profile	Debris smoke trail photograph
AB/AD	0.14	0.14
AC/AD	0.49	0.53
BC/AD	0.35	0.40
BD/AD	0.86	0.86
CD/AD	0.51	0.47

TABLE 3. Mean wind analysis.

	$\bar{v}_2 - \bar{v}_1$	$\Delta\bar{D}/\Delta z$
L + 9 min profile	16.5 m s^{-1}	0.229 (Eq (10)) 0.179 (corrected)
Photograph	17.1 m s^{-1}	0.186

where:

t_p = time of photograph after failure; i.e., 169 sec,
t_f = time of debris passage at 11.280 km; i.e., 75 sec,
$\bar{v}_1$ = mean wind between 11.280 km and 14.024 km (rawinsonde),
$\bar{v}_2$ = mean wind between 6.707 km and 11.280 km (rawinsonde),
$(\Delta\bar{D})_{\text{wind profile}} = (\bar{v}_2 - \bar{v}_1)(t_p - t_f)$,
$(\Delta z)_{\text{wind profile}} = 6.555$ km,
$(\Delta\bar{D})_{\text{photo}} = 0.8$ cm,
$(\Delta z)_{\text{photo}} = 4.3$ cm.

b. *Mean meridional winds*

The differential in mean drift provides information about the mean meridional wind differential mentioned earlier. According to Eq. (9), the difference between the vertically-averaged displacements $\bar{D}$ for the two layers at the time of the photograph in Fig. 6 is given by

$$\Delta\bar{D}/\Delta z = (\bar{v}_2 - \bar{v}_1)(t_p - t_f(11.280\text{ km}))/\Delta z, \quad (10)$$

where we have scaled $\Delta\bar{D}$ with the distance $\Delta z = AD = 6.555$ km. Using $t_p = 169$ s (elapsed time after failure) and $t_f(11.28\text{ km}) = 75$ s, which respectively represent the time of the photograph and the time of passage of the piece of debris at 11.28 km after the explosion, we can calculate the right side of Eq. (10) with the L + 9 min wind profile and the left side with the smoke trail photograph. Furthermore, we use Eq. (10) to estimate $\bar{v}_2 - \bar{v}_1$ from the photograph. The results of these calculations are presented in Table 3. The corrected entry in the table for the L + 9 min profile accounts for the overestimate in the horizontal drift of 300 m in the layer below 11.28 km. The results indicate a difference of approximately 4% between the L + 9 min and the smoke trail mean meridional wind differentials.

c. *Derived meridional wind profiles*

In this section we derive estimates of the meridional gust or wind perturbation profile and the total meridional wind profile. The third term on the right side of Eq. (9) is the perturbation in drift which we denote as $D'(z)$. This function has been estimated from the trail photograph at 169 sec after failure (Fig. 6) by subtracting the mean vertically-averaged horizontal trail coordinate above and below 11.28 km from the trail coordinate at any given altitude. An estimate of the meridional wind perturbation profile is obtained from the equation

$$v'(z) = D'(z)/(t_p - t_f(z)). \quad (11)$$

Figure 12 provides the perturbation meridional wind profile obtained by substituting our estimate of $D'(z)$ into Eq. (11). Addition of the L + 9 min mean winds ($\bar{v}_1 = -4.6$ m s^{-1}, $\bar{v}_2 = 11.9$ m s^{-1}) to our estimate of $v'(z)$ yields the total meridional wind profile in Fig. 7.

4. Statistical considerations

Differences between the L + 9 min and plume-derived winds can result from 1) not sampling the same volume of air and 2) measurement errors. The rawinsonde used to measure the L + 9 min profile was initiated at 9 min after launch and attained 10.67 km altitude at approximately 35 min after the launch of

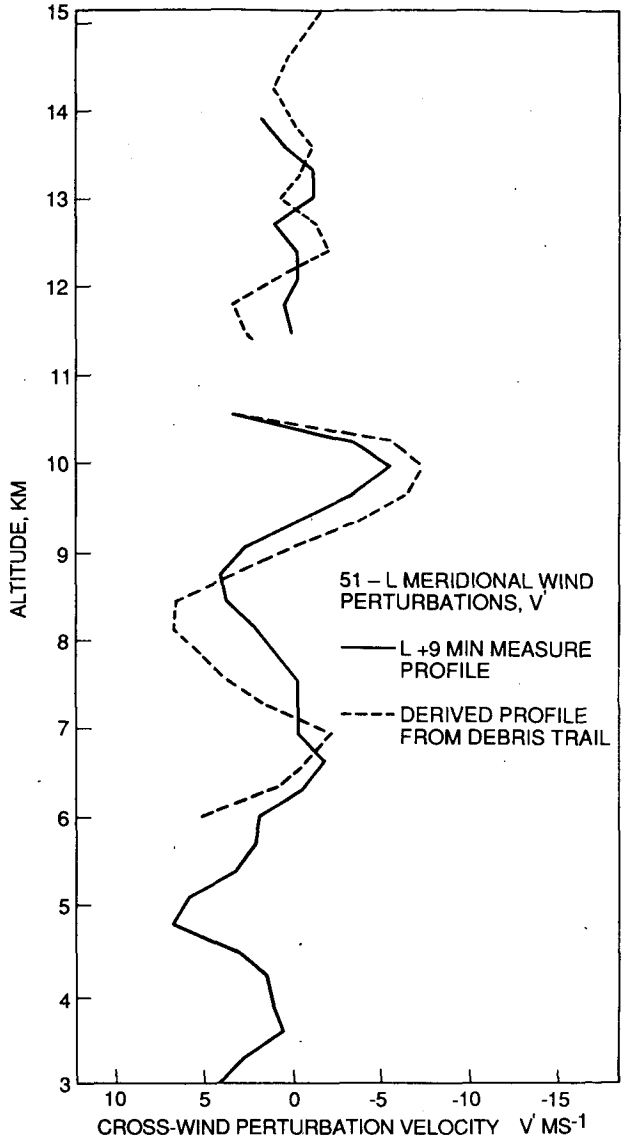

FIG. 12. A comparison of the L + 9 min measured perturbation wind profile and the perturbation wind profile obtained from debris smoke trails.

51-L. The exhaust and debris smoke trails used in this analysis were observed within the first two to three min after launch. The L + 9 min balloon drifted approximately 125 km downstream by the time it reached 10.67 km. On the other hand, the debris smoke trail at 10.67 km altitude was located at approximately 158 km east of the pad when the rawinsonde reached the same altitude. Accounting for time differences, the parcel of air at 10.67 km measured by the rawinsonde was approximately 33 km upstream from the air parcel associated with the debris trail. (The debris trail at 10.67 km altitude was approximately 6 km downstream from the air parcel in which 51-L flew.) The scales of motion with horizontal wavelength less than or equal to the horizontal distance (i.e., 33 km) between the smoke trail and rawinsonde profiles contribute to the rms velocity difference between the profiles. To estimate this difference, we use the L − 3.25 h and L + 3.5 h Jimsphere profiles and assume the associated vertical scales of motion are equal to one-tenth the horizontal scale. Accordingly, the L − 3.25 h and L + 3.5 h Jimsphere profiles were high-pass filtered with a cutoff wavelength (i.e., half-power point) equal to 3.3 km. The associated meridional velocity component variances were calculated to yield a meridional standard deviation $\sigma_v = 2.3$ m s^{-1} and the corresponding rms velocity difference is $\sigma_\Delta = \sqrt{2}\sigma_v = 3.3$ m s^{-1}.

The rawinsonde velocity component standard error depends on the wind profile that is being measured and the range and elevation and azimuth angle standard errors. Using well known rawinsonde error characteristics estimated with rawinsondes we estimate a meridional component measurement standard error $\sigma_r = 2$ m s^{-1}.

The mean meridional velocity differential derived from the debris smoke trail was larger than the measured L + 9 min value by 4%, or 0.6 m s^{-1}. The rms meridional standard deviation σ_0 which characterizes the distance effect and the rawinsonde measurement errors for the meridional velocity component measurements is given by $\sigma_0 = 4.3$ m s^{-1}. (This assumes that the standard error of measurement of the debris-derived profile is comparable to the standard error for the rawinsonde.) To estimate the corresponding standard deviation for the mean meridional wind differential, we multiply by 0.87 to obtain 3.8 m s^{-1}. This factor accounts for the effective sample size which goes into each part of the mean wind differential (i.e., effective sample size of two for $\bar{v}_1$ and 4 for $\bar{v}_2$). Estimation of effective sample size accounts for correlation along the vertical. The departure of 0.7 m s^{-1} in the mean meridional velocity differentials associated with the debris- and rawinsonde-derived winds can be accounted for by the distance effect and rawinsonde errors.

Concerning the meridional velocity component perturbations, the departures of the smoke trail estimates from the rawinsonde values range from −4.5 m s^{-1} at 7.9 km to 1.5 m s^{-1} at 10.1 km. These perturbations fall within the $\sigma_0 = 4.3$ m s^{-1} envelope, so that we can explain the departures between the two gust profiles by the combined effects of distance between measurement points and the errors of measurement.

a. Shear

A comparison of the shear values associated with 51-L and a large population of Jimsphere and rawinsonde soundings (Table 4) suggests that the 51-L shear data is reasonable. Shown in Table 4 is a collection of shear intervals in meters, and for each of these intervals, the altitude for which the shear is largest. The maximum shear for this layer is given, plus the wind speed at the top of the layer. The probability that a randomly chosen shear from a population of 150 Jimsphere balloon launches for the month of January is less than or equal to the given shear is shown in the column "shear probability." Extreme values in this population are ob-

TABLE 4. Extreme largest wind speed shear versus shear interval.

Δz Shear interval (m)	z Altitude (m)	Δv Speed shear (m/s)	v Speed (m/s)	Shear probability (%)	Cond shear probability (%)
L − 4.5 h (Jimsphere)					
200	11525	5.68	50.52	37	30
400	11825	8.51	54.84	50	39
600	11925	12.00	56.84	65	46
800	12000	13.49	57.82	60	45
1000	12275	15.35	59.87	61	46
2000	12350	20.37	60.29	59	34
3000	12100	21.64	59.91	40	17
4000	12350	28.29	60.29	60	25
5000	13200	29.86	60.98	59	25
L + 9 min (Rawinsonde)					
400	11275	5.85	39.58	2	10
600	11275	8.40	39.58	5	28
800	11475	10.80	41.97	36	40
1000	11675	12.66	43.84	41	45
2000	12675	20.59	51.77	59	47
3000	12800	21.59	53.02	43	27
4000	14025	19.84	51.50	19	7
5000	14325	18.14	50.90	6	6
L + 3.5 h (Jimsphere)					
200	12475	7.41	43.84	75	75
400	11400	9.17	35.04	60	60
600	11400	9.07	35.04	36	37
800	12475	12.13	43.84	46	50
1000	12650	12.47	44.16	40	45
2000	12625	17.62	44.44	44	48
3000	13975	20.25	45.87	36	32
4000	14700	21.34	47.24	24	23
5000	15100	21.02	45.90	15	20

tained using a Gumble distribution. The probability that a randomly chosen shear is less than or equal to the given shear, for that portion of the population in which the wind speed exceeds the value given, is shown in the column labeled "conditional probability." For the Jimspheres, the shear probability tends to be greater than the conditional probability, and both probabilities tend to be larger for moderate shear. An exception to this is the larger percentage for a 200 m and a 400 m shear interval for the L + 3.5 h sounding. The rawinsonde, on the other hand, exhibited conditional shear probabilities that were larger than the shear probabilities. It is clear, however, that the shears obtained from the 51-L wind profiles are in the range expected if these measured shears were selected at random from the populations.

Of some possible concern is the exceedingly small shear probabilities for the L + 9 min (rawinsonde) profile in Table 4. An explanation for this anomaly is the inherent filtering of the data by the balloon and instrument system, as shown in Fig. 13. Wavelengths shorter than several hundred meters are severely damped by the rawinsonde system, but are well resolved by the Jimspheres.

b. Gusts

The wind gust data for 51-L was obtained from the Jimsphere soundings at L − 4.5 h and L + 3.5 h. The raw data was high-pass filtered to remove secular trends and eddies of wavelengths longer than 1500 m. The gust record was analyzed by counting the number of times the gust record trace crossed each given gust level with a positive slope. A cumulative distribution of the gust velocities was obtained and the percent of gust samples that exceeded a given velocity are plotted in Fig. 14. The head-tail percent exceedances are greater than the crosswind percent exceedances; however, these gust values fall within the design criteria for the shuttle.

5. Summary

The television data of the STS 51-L accident provided useful information for corroborating the rawinsonde wind profiles measured 9 min after launch. All noted differences between the quantities derived from television pictures of the STS 51-L launch and the L + 9 min profile can be explained by the measurement sites not being in the same location relative to the atmosphere and the standard errors associated with the measurement techniques.

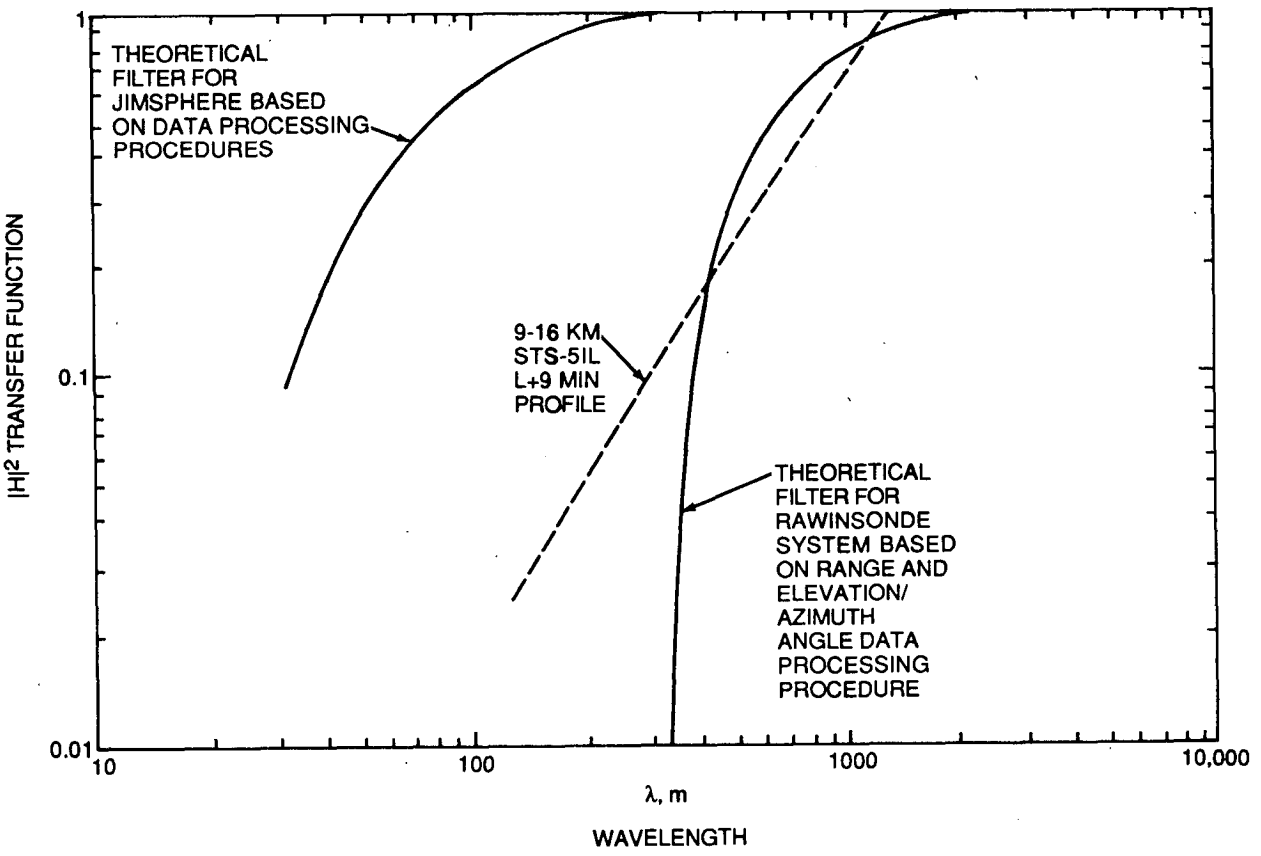

FIG. 13. The theoretical transfer function as a function of wavelength for the Jimsphere-based and rawinsonde-based data processing procedures.

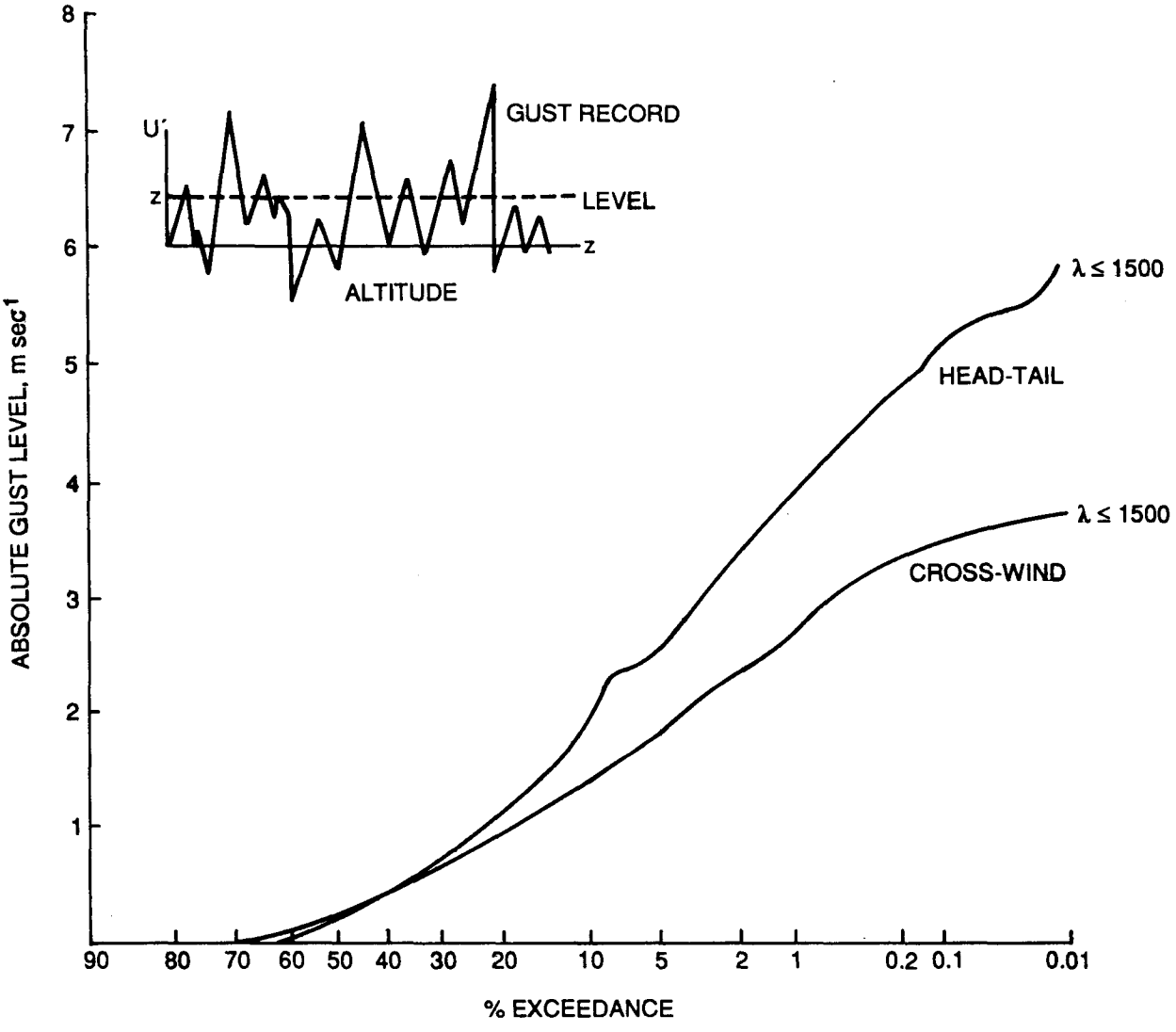

FIG. 14. The percent exceedance for the gust record as a function of the gust level for the head-tail winds and for the crosswinds.

REFERENCES

Fichtl, G. H., 1971: The response of rising or falling spherical wind sensors to atmospheric wind perturbations. *J. Appl. Meteor.*, **10**, 1275–1284.

——, R. E. DeMandel and S. J. Krivo, 1972: Aerodynamical properties of spherical balloon wind sensors. *J. Appl. Meteor.*, **11**, 472–481.

Tolefson, H. B., and R. M. Henry, 1961: A method of obtaining detailed wind shear measurements for application to dynamic response problems of missile systems. *J. Geophys. Res.*, **66**, 2849–2862.

Uccellini, L. W., K. F. Brill, R. A. Petersen, D. Keyser, R. Aune, P. J. Kocin and M. des Jardins, 1986: A report on the upper-level wind conditions preceding and during the Shuttle Challenger (STS 51L) explosion. *Bull. Am. Meteor. Soc.*, **67**, 1248–1265.